ACS NANO
Cite This: ACS Nano 2017, 11, 12257−12265
www.acsnano.org

ARTICLE

Valley Polarization of Trions and Magnetoresistance in Heterostructures of MoS_2 and Yttrium Iron Garnet

Bo Peng,*[,†] Qi Li,[†,#] Xiao Liang,[†,#] Peng Song,[‡] Jian Li,[†] Keliang He,[∥] Deyi Fu,[‡] Yue Li,[†] Chao Shen,[§] Hailong Wang,[§] Chuangtang Wang,[†] Tao Liu,[⊥] Li Zhang,[†] Haipeng Lu,[†] Xin Wang,[†] Jianhua Zhao,[§] Jianliang Xie,[†] Mingzhong Wu,[⊥] Lei Bi,*[,†] Longjiang Deng,*[,†] and Kian Ping Loh*[,‡]

[†]National Engineering Research Center of Electromagnetic Radiation Control Materials and State Key Laboratory of Electronic Thin Films and Integrated Devices, School of Microelectronics and Solid State Electronics, University of Electronic Science and Technology of China, Chengdu 610054, China

[‡]Department of Chemistry and Centre for Advanced 2D Materials and Graphene Research Centre, National University of Singapore, 3 Science Drive 3, Singapore 117543

[§]State Key Laboratory of Superlattices and Microstructures, Institute of Semiconductors, Chinese Academy of Sciences, Beijing 100083, China

[⊥]Department of Physics, Colorado State University, Fort Collins, Colorado 80523, United States

[∥]IBM, Malta, New York 12020, United States

Supporting Information

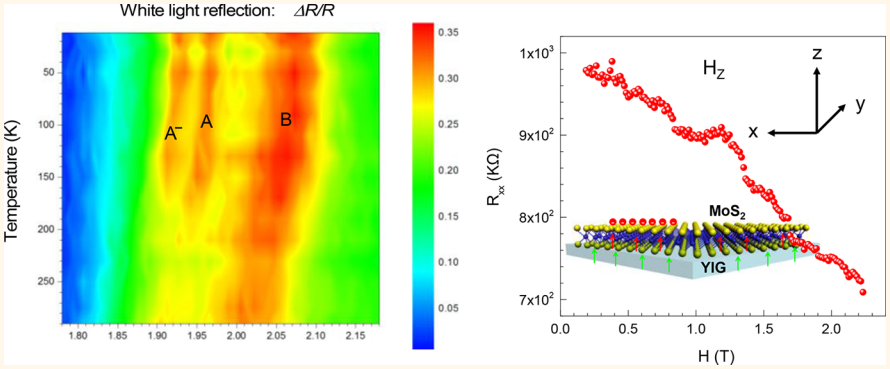

ABSTRACT: Manipulation of spin degree of freedom (DOF) of electrons is the fundamental aspect of spintronic and valleytronic devices. Two-dimensional transition metal dichalcogenides (2D TMDCs) exhibit an emerging valley pseudospin, in which spin-up (-down) electrons are distributed in a +K (−K) valley. This valley polarization gives a DOF for spintronic and valleytronic devices. Recently, magnetic exchange interactions between graphene and magnetic insulator yttrium iron garnet (YIG) have been exploited. However, the physics of 2D TMDCs with YIG have not been shown before. Here we demonstrate strong many-body effects in a heterostructure geometry comprising a MoS_2 monolayer and YIG. High-order trions are directly identified by mapping absorption and photoluminescence at 12 K. The electron doping density is up to ~10^{13} cm^{-2}, resulting in a large splitting of ~40 meV between trions and excitons. The trions exhibit a high circular polarization of ~80% under optical pumping by circularly polarized light at ~1.96 eV; it is confirmed experimentally that both phonon scattering and electron−hole exchange interaction contribute to the valley depolarization with temperature; importantly, a magnetoresistance (MR) behavior in the MoS_2 monolayer was observed, and a giant MR ratio of ~30% is achieved, which is 1 order of magnitude larger than the reported ratio in $MoS_2/CoFe_2O_4$ heterostructures. Our experimental results confirm that the giant MR behaviors are attributed to the interfacial spin accumulation due to YIG substrates. Our work provides an insight into spin manipulation in a heterostructure of monolayer materials and magnetic substrates.

KEYWORDS: *magnetic heterostructures, spintronics, valleytronics, valley polarization, 2D materials*

The Bloch states are strongly dependent on the crystal symmetry.[1−3] The monolayer transition metal dichalcogenides (TMDCs), such as MoS_2, $MoSe_2$, WS_2, and

Received: August 15, 2017
Accepted: November 28, 2017
Published: November 28, 2017

ACS Publications © 2017 American Chemical Society

DOI: 10.1021/acsnano.7b05743
ACS Nano 2017, 11, 12257−12265

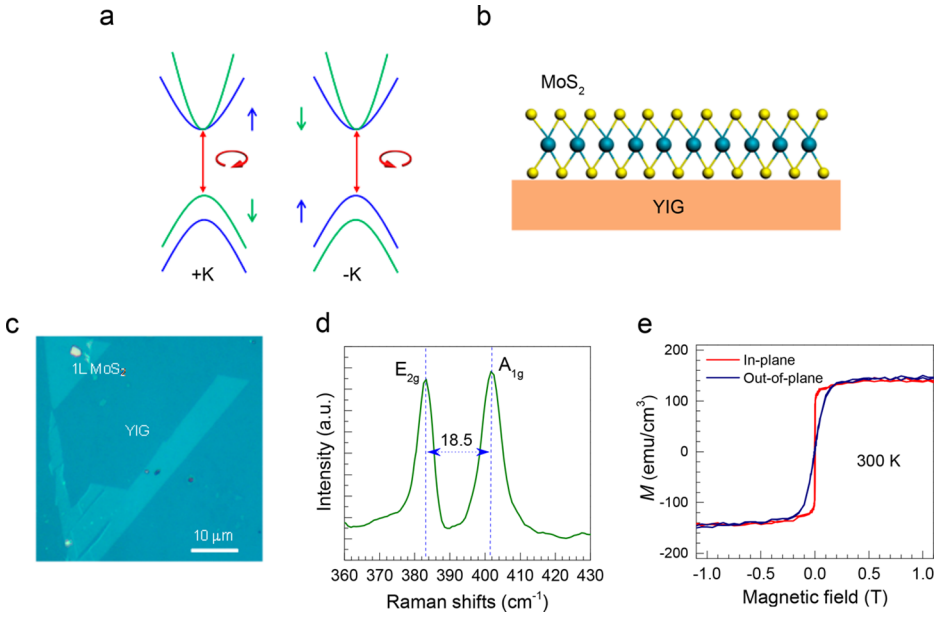

Figure 1. MoS_2/YIG heterostructure and optical selection rules at the +K (−K) point. (a) Schematic of valley and spin optical transition selection rules at the K and K′ points in the crystal momentum space. The bands of the same electron spin are in the same color. The spin degeneracy at the valence-band edges is lifted by spin−orbit interactions. The valley and spin degrees of freedom are coupled. The right- (left-) hand circular polarized light $\sigma-$ (σ^+) generates spin-up (-down) electrons and spin-down (-up) holes in the +K (−K) valley. (b, c) Schematic and optical image of a monolayer MoS_2/YIG heterostructure. (d) Raman spectra of monolayer MoS_2 on the YIG substrate. (e) Magnetization M of ∼60 nm YIG films on a Si substrate as a function of magnetic field at ∼300 K. The out-of-plane and in-plane saturation magnetization M_s are ∼0.2 and ∼0.01 T, respectively.

WSe_2, is half a unit cell of the bulk crystal and thus induces the breaking of space-reversal inversion symmetry. Two sublattices are occupied by one transition metal atom and two chalcogen atoms in the honeycomb lattice structure, thus generating a local in-plane electric field.[4] This gives rise to optical selection rules for interband transitions at the +K (−K) momentum valley and the valley Hall effect.[5−10] The spin-up (-down) electrons and spin-down (-up) holes mostly exist in the +K (−K) momentum valley under optical pumping by right-handed (left-handed) polarized light (Figure 1a). The orbital magnetic moment μ_l ($2\tau\mu_B$), the spin magnetic moment μ_s ($2s_z\mu_B$), and the valley magnetic moment μ_v ($\Delta\alpha\tau\mu_B$) contribute to the total magnetic moment μ of electrons (holes), which is perpendicular to the MoS_2 monolayer,[11,12] where μ_B is the Bohr magneton, $\tau = \pm 1$ for the ±K valleys, s_z is the spin in the z direction, $\alpha = m_0/m^*$, where m^* is the effective mass of electrons (holes) in the conduction (valence) band, and $\Delta\alpha = \alpha_c - \alpha_v$. Thus, the band gap should be increased in the +K momentum valley under a positive magnetic field ($B > 0$) and contrarily decreased in the −K momentum valley,[13] and the band gap shift $\Delta E = \mu B = -(2 - \Delta\alpha)\,\mu_B B$. The magnetic manipulation of valley splitting, however, is only feasible under high external magnetic field (B = ∼7 T).[11]

The interfacial magnetic exchange field can enhance the interaction of the total magnetic moment of electrons with the external magnetic field.[14−18] The ferromagnetic insulators, such as EuS and yttrium iron garnet (YIG), have given rise to the strong magnetic proximity effects, imparting ferromagnetic properties and an anomalous Hall effect in graphene, WSe_2, and Pt films.[16−18] However, the low Curie temperature (T_C = ∼15 K) and large saturation magnetization (M_s = ∼2 T) inherent in EuS thin films limit practical applications. The T_C of YIG films is above room temperature and the M_s is ∼0.2 T, which is critical for spin manipulation at high temperature and low magnetic field.[19] However, the interface physics of 2D TMDCs with YIG films have not been explored before. This raises two fundamental questions in the MoS_2/YIG heterostructure: (1) How do the YIG magnetic substrates affect the photoluminescence (PL) and valley polarization of a MoS_2 monolayer? and (2) do the magnetoresistance effect and interfacial magnetic exchange field take place in the MoS_2 monolayer? Moreover, in theory, the valley-spin relaxation originates from the electron−hole exchange interaction;[20−22] however, few experimental reports exist on the relaxation mechanism of valley polarization as a function of temperature.[23] Here we investigate the optical response and valley polarization of monolayer MoS_2 in a MoS_2/YIG heterostructure by means of absorption and photoluminescence spectroscopy. We demonstrate that the high electron doping of ∼10^{13} cm^{-2} gives rise to the trions in the whole MoS_2 monolayer. The splitting between trion resonance and neutral exciton A resonance is distinct below 170 K, which is ∼40 meV. The valley polarization of trions is ∼80% at 12 K. Our results experimentally demonstrate that the synergy of phonon-assisted intervalley scattering and electron−hole exchange interaction contributes to the valley depolarization with increasing temperature. Importantly, a giant magnetoresistance (MR) ratio of ∼30% is observed in MoS_2/YIG heterostructures. Both valley polarization and linear Hall resistance results exclude the possibility of an interfacial magnetic exchange interaction; thus the MR behaviors originate from the spin accumulation at the interface of the MoS_2 monolayer and YIG substrates.

RESULTS AND DISCUSSION

Trions in the MoS_2/YIG Heterostructure. In our investigation, MoS_2 monolayers were mechanically exfoliated from bulk crystal onto polydimethylsiloxane (PDMS) films and transferred onto ∼60 nm YIG films on a Si substrate. The MoS_2/YIG heterostructure is shown in Figure 1b and c. The Raman in-plane $E_{2g}{}^1$ mode and out-of-plane A_{1g} mode of the exfoliated

DOI: 10.1021/acsnano.7b05743
ACS Nano 2017, 11, 12257−12265

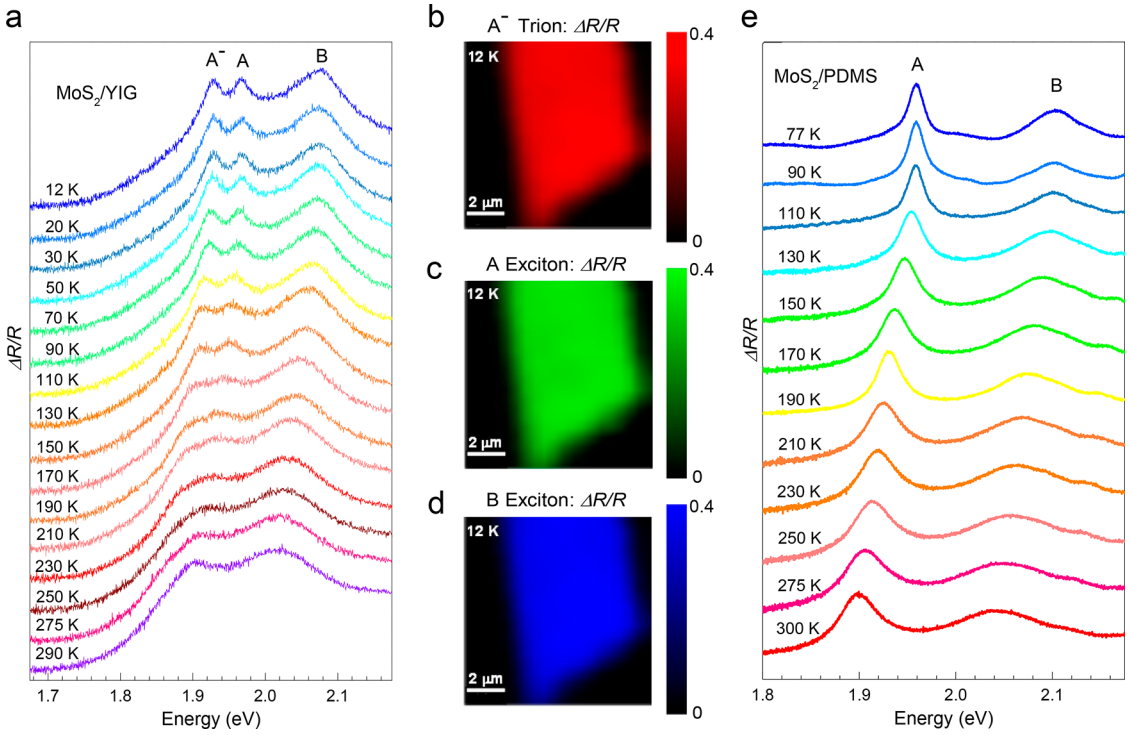

Figure 2. Electronic structure of the MoS_2 monolayer. (a) Absorption spectra of the MoS_2 monolayer as a function of temperature in the range of 12−290 K. The trion and exciton (A and B) resonances are noticeable and clearly distinguishable. (b, c, d) Absorption maps of trion and exciton (A and B) resonances of the MoS_2 monolayer on a YIG substrate at 12 K. This unambiguously demonstrates that trion resonances are uniformly formed in the MoS_2/YIG heterostructure. (e) Absorption spectra of the MoS_2 monolayer on PDMS substrates as a function of temperature, which do not offer any detectable trion feature.

MoS_2 monolayer are at 383.3 and 401.8 cm^{-1}, respectively (Figure 1d). The energy difference between E_{2g}^1 and A_{1g} modes is used extensively in the literature as the fingerprint of the number of layers, in this case the energy difference between the E_{2g}^1 and A_{1g} is 18.5 cm^{-1}, confirming that MoS_2 is a monolayer.[24−27] The YIG film is pure polycrystalline garnet phase (Supplementary Figure S1). The out-of-plane (hard axis) and in-plane (easy axis) M_s of the YIG films are ∼0.2 and 0.01 T at room temperature (Figure 1e), respectively, which highlights the feasibility of applying a low magnetic field toward the interfacial magnetic exchange field at high temperature.

The optical absorption spectra of an atomically thin monolayer allow us to gain an understanding of the basic features of the exciton in the MoS_2/YIG heterostructure. The strong spin−orbit coupling of the electrons in d-orbitals of the metal atoms results in the splitting of the valence band at the K points, giving rise to exciton A and B resonances in the band-edge transition. Figure 2a shows the typical absorption spectra of a MoS_2 monolayer as a function of temperature in the range of 12−290 K. It shows three pronounced absorption features at 12 K. The feature at 2.08 eV is associated with direct optical transitions of B excitons. Because of the electron doping, two peaks at 1.97 and 1.93 eV are identified, which are attributed to neutral A exciton resonance and a negatively charged trion resonance, respectively.[28−31] To further validate the trions in the MoS_2 monolayer, microabsorption mapping was performed at 12 K. All optical absorption measurements were carried out in a vacuum with ∼500 nm spatial resolution in the photon energy range of 1.6−2.2 eV. Figure 2b−d show the corresponding absorption intensity image of the trion, exciton A, and exciton B at 12 K, which visualize that the MoS_2 monolayer is homogeneously doped by electrons (Supplementary Figure S3a), giving rise to a trion accompanied by exciton A and exciton B across the whole MoS_2 monolayer. Below 170 K, the absorption features of trion and exciton A are distinct, which however are broadened as the temperature increases and become almost indistinguishable above 190 K (Figure 2a and Supplementary Figure S2). All three absorption resonances of the trion, exciton A, and exciton B are red-shifted as the temperature increases, which contributes to the interaction of electrons with optical phonons resulting from the high-frequency Bose−Einstein oscillations, in which $E(T) = E_0 + 2A_1/(\exp(E_1/k_BT) - 1) + A_1$, where E_1 is the average energy of the Bose−Einstein oscillators corresponding to the optical phonons (Supplementary S3). The temperature variation of the trion, exciton A, and exciton B can be well fitted by the Bose−Einstein oscillator model (Supplementary Figure S3b). The average energy of the optical phonons of the MoS_2 monolayer is ∼23 ± 4 meV. The splitting $\Delta E_{ex\text{-}tr}$ between the trion and exciton A is ∼40 ± 2 meV, which is almost independent of the temperature (Supplementary Figure S3b). Furthermore, to verify the electron doping from YIG substrates, we studied the absorption properties of the MoS_2 monolayer on PDMS substrates, which are used to exfoliate the corresponding MoS_2 monolayer (Figure 2e). The exciton A and B features are clearly detected; however, no detectable trion feature is observed; this indicates that YIG substrates contribute to the electron doping toward the trions. We speculate that the electron doping for trions may be due to the oxygen dangling bonds on the surfaces of YIG substrates ($Y_3Fe_5O_{12}$).

Valley Polarization of Trions. The temperature dependence of trion PL intensity yields insight into the trion binding energy. We photoexcite a MoS_2/YIG heterojunction by a right-hand (σ^-) and left-hand (σ^+) circular polarized laser at 1.96 eV, giving rise to a right-hand (σ^-) and left-hand (σ^+) circular

DOI: 10.1021/acsnano.7b05743
ACS Nano 2017, 11, 12257−12265

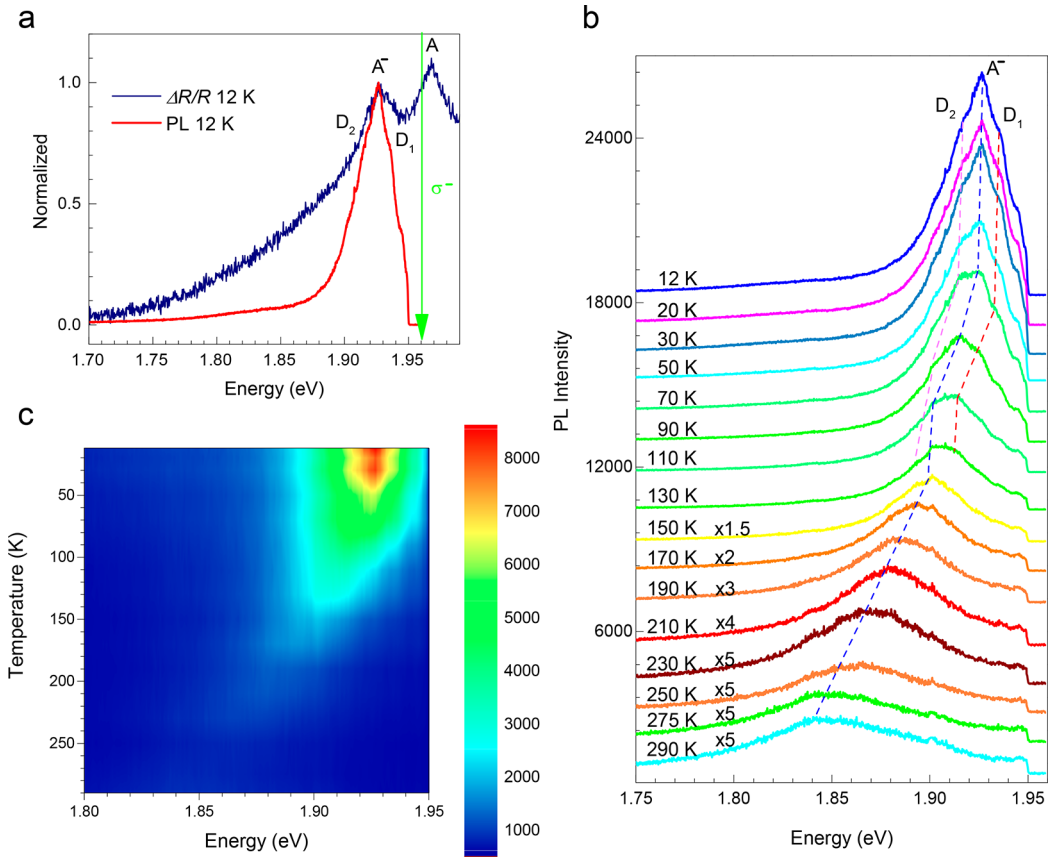

Figure 3. Valley and spin control of trions as a function of temperature. (a) Absorption and right-hand circular PL emission (σ^-) spectra of monolayer MoS_2 at 12 K. The green arrow represents the photon energies at 1.96 eV used to excite the samples in the circular PL measurements. (b) Right-hand circular emission (σ^-) spectra as a function of temperature by right-hand (σ^-) circularly polarized excitation at 1.96 eV. (c) Two-dimensional image of right-hand circular emission (σ^-) in (b).

emission. It should be noted that the excitation energy is smaller than the A exciton resonance energy below 90 K (Supplementary Figure S3b). Figure 3a shows the right-hand PL and corresponding absorption spectra of the MoS_2 monolayer in a MoS_2/YIG heterojunction at 12 K. The PL peak at ~1.93 eV matches the trion absorption resonance in both its position and width. Therefore, we attribute the PL emission to the trions.[32] We attribute the feature at 1.92 and 1.94 eV to the emission of defect-trapped excitons.[20,33] The evolution of the trion emission energy as a function of the temperature under a right-hand circular polarized laser at 1.96 eV with 1.5 mW is plotted in Figure 3b,c. As the temperature increases from 12 K to 290 K, the PL peak energy monotonically decreases from 1.93 eV to 1.85 eV. The trion binding energy (ΔE_{trb}) is estimated to be ~17 ± 2 meV (Supplementary Figure S4),[34] which is comparable with the reported value.[30] The two PL peaks at 1.92 and 1.94 eV become weak as the temperature increases and are almost indistinguishable and disappear above 150 K. We suggest thus that the PL emission at 1.92 and 1.94 eV may be due to the defects in the MoS_2 monolayer. The trion binding energy ΔE_{trb} is predicted to obey $\Delta E_{trb} = \Delta E_{ex\text{-}tr} - 0.5(m_{ex}/m_{trb})E_f$,[29] where $m_{trb} = 2m_e + m_h = 1.13m_0$ and $m_{ex} = m_e + m_h = 0.78m_0$, where m_0 is the effective mass in units of electron mass of the MoS_2 monolayer.[35] Thus, the Fermi energy E_f is ~67 meV in the MoS_2/YIG heterojunction. In atomically thin 2D materials, the size confinement and weak screening result in a dramatically enhanced exciton effect, electron–electron interactions, and Coulomb interactions.[30] The Coulomb potential for electrons and holes separated by a distance of r is defined by $V_{eff}(2D) \propto -\frac{1}{r_0}\left(\ln\left(\frac{r}{r+r_0}\right) + (\gamma - \ln 2)e^{-r/r_0}\right)$, where r_0 is the screening length, which is ~3–4 nm in 2D materials, and γ is the Euler's constant, ~0.5772.[36−38] Importantly, the dimensionless strength of the charge interactions, r_s, can be considered to be the ratio of Coulomb potential to kinetic energy, which is given by $r_s = 2/\sqrt{\pi n}(\varepsilon_{eff}\hbar^2/m_e e^2)$. Thus, the Coulomb potential of the MoS_2 monolayer is an order of magnitude larger than that of 2DEG system at the conventional heterojunctions, which also increases as a function of electron density (Supplementary S5, Figure S5).[30,39] To clearly compare with recently reported results, we still use the Fermi level equation from ref 31, $E_f = \hbar^2\pi n_e/2m_e e^2$, although which is more appropriate for a 2D electron gas in GaAs semiconductor heterojunctions; the electron density n_e is thus estimated to be ~1.0×10^{13} cm^{-2}, which is comparable with the reported value achieved under an 80 V gate voltage.[30] However, it should be noted that the effective electron mass m_e is from the MoS_2 monolayer, and thus the obtained n_e can still be used to measure the electron density in the MoS_2 monolayer to some extent.

Further, our polarization-resolved PL shows that the luminescence of trions conserves valley polarization. The right and left circularly polarized luminescence spectra of trions in a MoS_2/YIG heterostructure at 12 K are shown in Figure 4a and b, respectively. Under the right-hand circular polarized (σ^-) excitation at 1.96 eV with 1.5 mW, the $P(\sigma^-)$ is much larger than $P(\sigma^+)$, and the degree of circular polarization η is ~70%, which is defined as $\eta = (P(\sigma^-) - P(\sigma^+))/(P(\sigma^-) + P(\sigma^+))$,

DOI: 10.1021/acsnano.7b05743
ACS Nano 2017, 11, 12257–12265

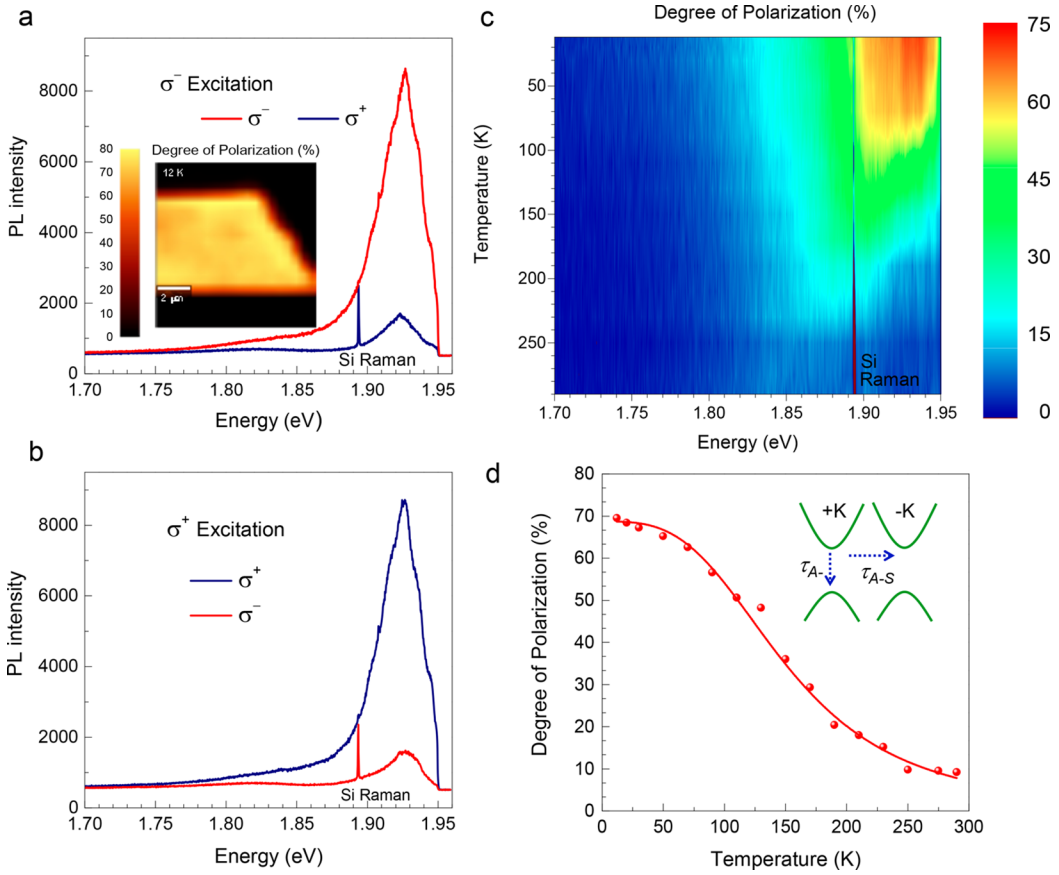

Figure 4. Valley depolarization mechanism. (a, b) Polarization-resolved photoluminescence spectra of the trions by right-hand (σ^-) and left-hand (σ^+) circular polarized excitation at 1.96 eV at 12 K, nearly on-resonance with the trion and A exciton. The peak at ~1.89 eV is assigned to a Si Raman feature, indicating that the system is in excellent calibration. The inset in (a) is a two-dimensional image of the degree of circular polarization η at 12 K; η = ~70%. (c) Degree of circular polarization η as a function of temperature in the range of 1.70−1.96 eV. (d) Temperature dependence of η of the trions. The inset represents the spin relaxation.

where $P(\sigma^-)$ and $P(\sigma^+)$ are the intensity of right-hand (σ^-) and left-hand (σ^+) circular polarized PL. The distinct sharp peak at ~1.89 eV in the left-hand PL spectra is the Raman signals of Si, however which is undetectable in the right-hand PL spectra, thus validating that our system is in good calibration for valley polarization measurement. The inset in Figure 4a shows the mapping of η of the corresponding MoS_2 monolayer on YIG substrates at 12 K, which indicates that the η is in the range of 70−80% in the MoS_2 monolayer.

Figure 4c show the temperature dependence of the degree of polarization η under right-hand circularly polarized excitation, which decreases as the temperature increases (Supplementary S6, Figure S6). Below 30 K, the η is nearly temperature independent with a similar value. In the MoS_2 monolayer, the Elliot−Yafet (EY) mechanism and the Dyakonov−Perel (DP) mechanism are strongly suppressed for spin relaxation, and the large spin splitting (0.5−1 eV) inhibits the intravalley spin flip.[20] The Bir−Aronov−Pikus (BAP) mechanism, which is due to the e−h exchange interaction, contributes to the spin-flip and intervalley scattering, which allows a hole spin to relax by a simultaneous valley- and spin-flip scattering with the electrons. The circular polarization η is equal to $P_0/(1 + 2\tau_{A-}/\tau_{A-S})$, where τ_{A-} is the PL lifetime and τ_{A-S} is the intervalley relaxation time of the trions (Figure 4d, inset). It is supposed that the intervalley electron−hole exchange interaction contributes to valley depolarization; on the other hand, the intervalley scattering involved in the Coulomb potential, phonons, and impurities also results in the valley depolarization.[21,22] It is hypothesized that the intervalley scattering relaxation rate $1/\tau_{A-S}$ is proportional to both the phonon population $1/e^{\hbar w/k_BT}$ and the electron−hole exchange interaction $k_BT\,(2m_hk_BT)^{1/2}$; the radiative lifetime of trions obeys a monotonically increasing relation with increasing temperature, $\tau_{RA-} \propto k_BT$;[20,40−43] on the contrary, the nonradiative time decreases with temperature, $\tau_{NRA-} \propto e^{E_a/k_BT}$.[44,45] The lifetime of trions thus is given by $1/\tau_{A-} \propto 1/k_BT + e^{-E_a/k_BT}$. We anticipate that the intervalley spin relaxation may be due to the combination of various mechanisms described above to some extent; thus the temperature variation of the degree of circular polarization of the trions is well fitted by $\eta \propto 1/(1 + bT^\alpha/(e^{\beta/T} + \gamma T))$ and $\alpha = 3.1$, which is close to the theoretical parameter of 2.5 (Figure 4d). Thus, the synergy of electron−hole exchange interaction and phonon scattering determines the temperature variation of valley polarization. It should be noted that the energy difference between the excitation laser (1.96 eV) and the trion resonance also increases as the temperature increases (Supplementary Figure S3b), which may also contribute to the decrease of valley polarization.[20]

The magnetic moment depends on the exchange coupling strength of different atoms from YIG and the adjacent layer. The YIG termination layer and defects contribute to the interfacial magnetic exchange, which also determines the electronic and magnetic properties of the adjacent layer, such as Pt and graphene.[46] We thus investigate the valley Zeeman splitting in heterostructures comprising a MoS_2 monolayer and YIG, GaMnAs, Eu-doping YIG, and YIG treated by Ar and O_2 plasma

DOI: 10.1021/acsnano.7b05743
ACS Nano 2017, 11, 12257−12265

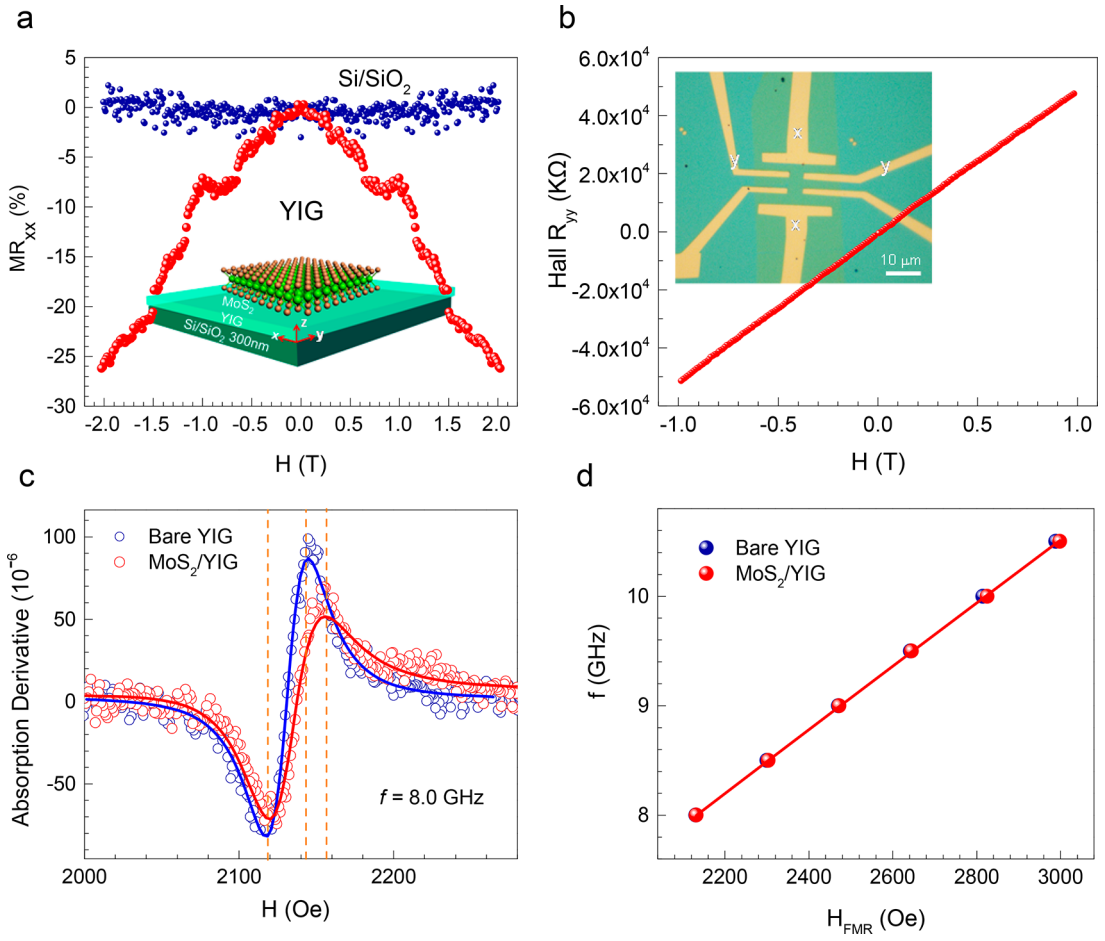

Figure 5. Magnetoresistance behaviors. (a) MR behaviors of a MoS_2 monolayer on YIG and SiO_2/Si substrates when the H_z is applied perpendicular to the electric current I_{xx} at 1.5 K. The inset is a schematic cartoon of the MoS_2/YIG device. (b) Total Hall resistivity under a gate voltage of 80 V at 1.5 K. The inset shows the device microscopy image. (c) FMR profile for a bare YIG (5 nm) sample and a MoS_2/YIG (5 nm) sample. The solid curves show Lorentzian fits. (d) FMR field (H_{FMR}) *vs* microwave frequency for bare YIG and MoS_2/YIG samples, which can be fitted well by $f = \gamma\sqrt{H(H + 4\pi M_s)}$, indicating $4\pi M_s$ = ~1678 ± 3 G.

under a magnetic field of ±0.2 T at 12 K. However, there is no distinguished difference between the right- and left-hand PL emission spectra (Supplementary S7, Figure S7). The first-principles calculation results show that the Zeeman splitting of MoS_2 can be neglected in a van der Waals heterostructure comprising a MoS_2 monolayer and a YIG terminated by a crystalline plane (111) consisting of tetrahedral and octahedral Fe^{3+} and Y^{3+} ions (Supplementary S8, Figure S8). Thus, we suggest that the Zeeman-type splitting is too weak to be observed in the MoS_2/YIG heterostructures at 0.2 T magnetic fields.

To validate interfacial spin interaction of a 2D TMDC monolayer and YIG magnetic insulator, the magnetoresistance of a MoS_2 monolayer on YIG substrates is studied at 1.5 K. As shown in the insets in Figure 5a and b, the longitudinal resistance of a MoS_2 monolayer on YIG substrates is given by $R_{xx} = V_{xx}/I_{xx}$ when the current (I_{xx}) flows along the longitudinal direction under the out-of-plane magnetic field (H_z), which is normal to the MoS_2 monolayer plane and perpendicular to the I_{xx}. The MR ratio (MR_{xx}) is defined by $(R_{xx}(H) - R_{xx}(0))/R_{xx}(0)$. A giant MR behavior is clearly observed at 1.5 K (Figure 5a). The resistance of the MoS_2 monolayer is decreased as the magnetic field increases. A negative MR_{xx} ratio thus is obtained and up to −26% under a 2 T magnetic field, which is 1 order of magnitude larger than that in $MoS_2/CoFe_2O_4$ heterostructures at least. Recently, negative MR behaviors have been observed in Dirac semimetal Cd_3As_2 nanowires and ribbons,[47,48] $TaSb_2$,[49] and $ZrTe_5$[50] and Weyl semimetals TaAs[51] and few-layer WTe_2[52] due to the chiral anomaly effect and the weak localization. A giant positive MR also has been detected in polycrystal graphene, which originates from the ripples formed at nanodomain boundaries.[53] However, no detectable MR behavior is observed in a single-crystal MoS_2 monolayer on Si/SiO_2 substrates (Figure 5a),[54] which indicates that the chiral anomaly, weak localization, and nanodomain boundary effect can be ruled out in the MoS_2/YIG heterostructures. It should be noted that the YIG and SiO_2 films are insulator materials, which cannot divert the electron current away from the MoS_2 monolayer; thus we speculate that the variation of resistance of the MoS_2 monolayer as a function of magnetic field is due to the interface spin interaction in MoS_2 and YIG. Generally speaking, two possible physical mechanisms determine the MR behaviors: (1) the induced magnetic moment by interfacial magnetic proximity effect; (2) accumulated spin at the interface, in which the spin-current is coupled with the electron current, leading to the resistance change. Since the right-hand and left-hand circularly polarized PL spectra are almost totally overlapped under a magnetic field correlated with the saturation magnetization of YIG (Figure 1e), this indicates that no magnetic proximity effect takes place at the interface of the

DOI: 10.1021/acsnano.7b05743
ACS Nano 2017, 11, 12257−12265

MoS_2 monolayer and YIG. The Hall effect measurements show a linear ordinary Hall resistance behavior (Figure 5b), which also indicates that proximity-induced magnetism can be ruled out, consistent with the polarization-resolved PL results. Thus, we attribute the negative MR behavior to the interfacial spin accumulation due to YIG.

To obtain an understanding of interfacial spin interaction mechanism, ferromagnetic resonances (FMR) were carried out in shorted waveguides and cavities. Figure 5c shows the FMR absorption derivative profiles of bare YIG and MoS_2/YIG heterostructures obtained with an 8.0 GHz cavity. The thickness of the YIG layer in both samples is tuned to be 5 nm for facilitating the observation of interfacial interaction.[55] The FMR line-width (ΔH) is assigned to be the peak-to-peak line-width of the FMR absorption derivative profiles, which is given by $\sqrt{3}\Delta H = 2\alpha f/|\gamma| + \Delta H_0$, where α is the effective damping parameter, f is the microwave frequency, $|\gamma|$ is the gyromagnetic ratio, $|\gamma| = 2.8$ MHz/Oe, and ΔH_0 represents the line-width inhomogeneity. The FMR peak-to-peak line-widths of YIG (ΔH_YIG) and MoS_2/YIG (ΔH_MoS_2/YIG) are 27.2 and 35.2 Oe, respectively. The larger line-width of MoS_2/YIG indicates an increasing damping and the occurrence of spin pumping and transfer of spin angular momentum between YIG and MoS_2 at the interface.[17] Compared with a ΔH enhancement of 74.2% and 193.5% in graphene/YIG and Pt/YIG,[17] a 29.4% enhancement of ΔH is absolutely observed in our MoS_2/YIG heterostructures, indicating lower but manifest interfacial coupling of spin angular momentum at the interface. The spin pumping is attributed to the interfacial coupling of the MoS_2 monolayer and spins in the YIG films,[55] which results in a torque between MoS_2 and YIG magnetization. This torque leads to an increase of the FMR line-width and simultaneously influences the resistivity and mobility of the MoS_2 monolayer and further results in the giant magnetoresistance. Figure 5d shows the FMR field (H_{FMR}) as a function of microwave frequency. The H_{FMR} of MoS_2/YIG and bare YIG are overlapped almost totally, which confirms that no magnetic proximity effect takes place again and may also rule out the static coupling of magnetization at the interface, consistent with the polarization-resolved PL and Hall resistance results. It is thus speculated that the interfacial spin coupling and accumulation contribute to the magnetoresistance behavior. Further systematic studies are needed on the other types of 2D TMDC monolayers (such as CrI_3 and $Cr_2Ge_2Te_3$), crystal stacking, defects, and gate voltage, which may play a significant role in defining the magnetic exchange interaction and interfacial spin manipulation.

CONCLUSION

Our studies reveal that the YIG magnetic insulator gives a doping electron density of $\sim 10^{13}$ cm^{-2}, giving rise to trions in the MoS_2 monolayer; the spin accumulation induces a giant magnetoresistance ratio of ~30% at the interface of the MoS_2 monolayer and YIG films, which derives from the torque due to spin interfacial coupling. The trions show high circular polarization and large binding energy, which may provide possibilities of the manipulation of many-body states of the TMDC monolayer. The electron doping density for trions also can be tuned from $\sim 5 \times 10^{12}$ cm^{-2} to $\sim 1 \times 10^{13}$ cm^{-2} by electric field under gate voltages from 0 to 80 V.[30] Our YIG was grown on p-doped Si substrates, which is facilitated to further deeply tune the trions to improve the splitting energy, developing integrated optoelectronic and photonic devices.

The time-reversal symmetry of 2D TMDCs is broken under optical excitation by circularly polarized light, which gives rise to the valley Hall effect.[56] The 2D TMDCs/YIG heterostructures show potential to give a magnetic freedom to manipulate the electron spin for spintronic and valleytronic devices by spin and valley Hall effects. Recently, YIG was shown to be an ideal material for spin-wave spin-currents, although it is an insulator for electric currents.[57] The spin-wave spin-current is injected from the YIG layer into the Pt layer, in which the spin-current is converted into an electric voltage perpendicular to the spin polarization direction *via* spin−orbital coupling.[58,59] Therefore, the 2D TMDCs/YIG heterostructures are a promising geometry toward spin-wave spin-current devices.

EXPERIMENTAL METHODS

Sample Preparation. MoS_2 monolayer flakes were mechanically exfoliated from bulk crystal onto PDMS films and then transferred onto YIG/Si substrates, which were grown by pulsed laser deposition.[19]

Optical Spectroscopy Measurement. The PL, Raman, and reflection signals were recorded by a Witec Alpha 300R Plus confocal Raman microscope, which is coupled with a closed cycle optical cryostat (10 K) and a XY scanning stage. A long work distance 50× objective (NA = 0.55) was used for the low-temperature PL and reflection measurement. The polarization-resolved PL spectra were obtained under a circular polarization excitation at 1.96 eV of 1.5 mW. The Raman spectra were collected under 2.33 eV laser excitation of 5 mW. The magnetic field of 0.2 T was home-built by a $Nd_2Fe_{14}B$ permanent magnetism disk with a ~1 cm diameter and ~1.3 mm thickness, and a hole of ~1 mm diameter is at the center of the disk. The sample was put between two $Nd_2Fe_{14}B$ disks through the hole, which were put in the cryostat.

Magnetoresistance Measurement. The magnetoresistance and Hall resistance measurements were performed in an Oxford Teslatron system at a base temperature of 1.5 K. All resistances were measured by sourcing a DC current of 10 nA with a Keithley 2400 and measuring the voltage signal using a Keithley 2000. A gate voltage of 80 V was supplied with a Keithley 6430.

ASSOCIATED CONTENT

Supporting Information

The Supporting Information is available free of charge on the ACS Publications website at DOI: 10.1021/acsnano.7b05743.

XRD spectrum of YIG; temperature variation of the electronic structure of monolayer MoS_2; Bose−Einstein oscillations and Varshin model; binding energy of trions; Coulomb potential of electrons and holes in 2D materials; temperature variation of degree of polarization of MoS_2 monolayer; circular PL emission spectra under a magnetic field of ±0.2 T; first-principles calculation in a van der Waals MoS_2/YIG heterostructure (PDF)

AUTHOR INFORMATION

Corresponding Authors

*E-mail: bo_peng@uestc.edu.cn.
*E-mail: bilei@uestc.edu.cn.
*E-mail: denglj@uestc.edu.cn.
*E-mail: chmlohkp@nus.edu.sg.

ORCID

Bo Peng: 0000-0001-9411-716X
Deyi Fu: 0000-0003-1365-8963
Jianhua Zhao: 0000-0003-2269-3963
Lei Bi: 0000-0002-2698-2829
Kian Ping Loh: 0000-0002-1491-743X

DOI: 10.1021/acsnano.7b05743
ACS Nano 2017, 11, 12257−12265

Author Contributions

[#]Q. Li and X. Liang contributed equally to this work. B.P. and L.B. conceived the idea and supervised the experiments. B.P. and D.F. prepared the MoS_2 monolayer and the MoS_2/YIG heterostructures. B.P., J.L, C.S., Y.L., and Q.L. carried out low-temperature PL, Raman, and reflection measurements. L.B. and C.W. grew the YIG films on Si substrate; X.L. carried out the first-principles calculation. T.L. and M.W. carried out the FMR characterizations. B.P. L.D., K.L., L.B., L.Z., H.L., J.X., and K.H. performed data analysis. All authors discussed the results and wrote the manuscript.

Notes

The authors declare no competing financial interest.

ACKNOWLEDGMENTS

We acknowledges financial support from Scientific Research Foundation for New Teachers of UESTC (A03013023601007), National Science Foundation of China (51602040, 61475031, 11404324, 51302027, and 51522204), and Ministry of Science and Technology of China MOST No. 2016YFA0300802

REFERENCES

(1) Ye, Y.; Xiao, J.; Wang, H.; Ye, Z.; Zhu, H.; Zhao, M.; Wang, Y.; Zhao, J.; Yin, X.; Zhang, X. Electrical Generation and Control of the Valley Carriers in a Monolayer Transition Metal Dichalcogenide. *Nat. Nanotechnol.* **2016**, *11*, 598−602.

(2) Wu, S.; Ross, J. S.; Liu, G. B.; Aivazian, G.; Jones, A.; Fei, Z.; Zhu, W.; Xiao, D.; Yao, W.; Cobden, D.; Xu, X. Electrical Tuning of Valley Magnetic Moment through Symmetry Control in Bilayer MoS_2. *Nat. Phys.* **2013**, *9*, 149−153.

(3) Wang, Z.; Shan, J.; Mak, K. F. Valley- and Spin-Polarized Landau Levels in Monolayer WSe_2. *Nat. Nanotechnol.* **2017**, *12*, 144−149.

(4) Jones, A. M.; Yu, H.; Ghimire, N. J.; Wu, S.; Aivazian, G.; Ross, J. S.; Zhao, B.; Yan, J.; Mandrus, D. G.; Xiao, D.; Yao, W.; Xu, X. Optical Generation of Excitonic Valley Coherence in Monolayer WSe_2. *Nat. Nanotechnol.* **2013**, *8*, 634−638.

(5) Xu, X.; Yao, W.; Xiao, D.; Heinz, T. F. Spin and Pseudospins in Layered Transition Metal Dichalcogenides. *Nat. Phys.* **2014**, *10*, 343−350.

(6) Rivera, P.; Seyler, K. L.; Yu, H.; Schaibley, J. R.; Yan, J.; Mandrus, D. G.; Yao, W.; Xu, X. Valley-Polarized Exciton Dynamics in a 2D Semiconductor Heterostructure. *Science* **2016**, *351*, 688−691.

(7) Cao, T.; Wang, G.; Han, W.; Ye, H.; Zhu, C.; Shi, J.; Niu, Q.; Tan, P.; Wang, E.; Liu, B.; Feng, J. Valley-Selective Circular Dichroism of Monolayer Molybdenum Disulphide. *Nat. Commun.* **2012**, *3*, 887.

(8) Xiao, D.; Liu, G.; Feng, W.; Xu, X.; Yao, W. Coupled Spin and Valley Physics in Monolayers of MoS_2 and Other Group-VI Dichalcogenides. *Phys. Rev. Lett.* **2012**, *108*, 196802.

(9) Peng, B.; Ang, P. K.; Loh, K. P. Two-Dimensional Dichalcogenides for Light-Harvesting Applications. *Nano Today* **2015**, *10*, 128−137.

(10) Lee, J.; Mak, K. F.; Shan, J. Electrical Control of the Valley Hall Effect in Bilayer MoS_2 Transistors. *Nat. Nanotechnol.* **2016**, *11*, 421−425.

(11) Aivazian, G.; Gong, Z.; Jones, A. M.; Chu, R.-L.; Yan, J.; Mandrus, D. G.; Zhang, C.; Cobden, D.; Yao, W.; Xu, X. Magnetic Control of Valley Pseudospin in Monolayer WSe_2. *Nat. Phys.* **2015**, *11*, 148−152.

(12) MacNeill, D.; Heikes, C.; Mak, K. F.; Anderson, Z.; Kormányos, A.; Zólyomi, V.; Park, J.; Ralph, D. C. Breaking of Valley Degeneracy by Magnetic Field in Monolayer $MoSe_2$. *Phys. Rev. Lett.* **2015**, *114*, 037401.

(13) Zhao, C.; Norden, T.; Zhang, P.; Zhao, P.; Cheng, Y.; Sun, F.; Parry, J. P.; Taheri, P.; Wang, J.; Yang, Y.; Scrace, T.; Kang, K.; Yang, S.; Miao, G. X.; Sabirianov, R.; Kioseoglou, G.; Huang, W.; Petrou, A.; Zeng, H. Enhanced Valley Splitting in Monolayer WSe_2 Due to Magnetic Exchange Field. *Nat. Nanotechnol.* **2017**, *12*, 757−762.

(14) Wei, P.; Lee, S.; Lemaitre, F.; Pinel, L.; Cutaia, D.; Cha, W.; Katmis, F.; Zhu, Y.; Heiman, D.; Hone, J.; Moodera, J. S.; Chen, C. T. Strong Interfacial Exchange Field in the Graphene/EuS Heterostructure. *Nat. Mater.* **2016**, *15*, 711−716.

(15) Dushenko, S.; Ago, H.; Kawahara, K.; Tsuda, T.; Kuwabata, S.; Takenobu, T.; Shinjo, T.; Ando, Y.; Shiraishi, M. Gate-Tunable Spin-Charge Conversion and the Role of Spin-Orbit Interaction in Graphene. *Phys. Rev. Lett.* **2016**, *116*, 166102.

(16) Lu, Y. M.; Choi, Y.; Ortega, C. M.; Cheng, X. M.; Cai, J. W.; Huang, S. Y.; Sun, L.; Chien, C. L. Pt Magnetic Polarization on $Y_3Fe_5O_{12}$ and Magnetotransport Characteristics. *Phys. Rev. Lett.* **2013**, *110*, 147207.

(17) Mendes, J. B. S.; Alves Santos, O.; Meireles, L. M.; Lacerda, R. G.; Vilela-Leão, L. H.; Machado, F. L. A.; Rodríguez-Suárez, R. L.; Azevedo, A.; Rezende, S. M. Spin-Current to Charge-Current Conversion and Magnetoresistance in a Hybrid Structure of Graphene and Yttrium Iron Garnet. *Phys. Rev. Lett.* **2015**, *115*, 226601.

(18) Wang, Z.; Tang, C.; Sachs, R.; Barlas, Y.; Shi, J. Proximity-Induced Ferromagnetism in Graphene Revealed by the Anomalous Hall Effect. *Phys. Rev. Lett.* **2015**, *114*, 016603.

(19) Bi, L.; Hu, J.; Jiang, P.; Kim, D. H.; Dionne, G. F.; Kimerling, L. C.; Ross, C. A. On-Chip Optical Isolation in Monolithically Integrated Non-Reciprocal Optical Resonators. *Nat. Photonics* **2011**, *5*, 758−762.

(20) Mak, K. F.; He, K.; Shan, J.; Heinz, T. F. Control of Valley Polarization in Monolayer MoS_2 by Optical Helicity. *Nat. Nanotechnol.* **2012**, *7*, 494−498.

(21) Yu, H.; Cui, X.; Xu, X.; Yao, W. Valley Excitons in Two-Dimensional Semiconductors. *Natl. Sci. Rev.* **2015**, *2*, 57−70.

(22) Yu, T.; Wu, M. W. Valley Depolarization due to Intervalley and Intravalley Electron-Hole Exchange Interactions in Monolayer MoS_2. *Phys. Rev. B: Condens. Matter Mater. Phys.* **2014**, *89*, 205303.

(23) Zeng, H.; Dai, J.; Yao, W.; Xiao, D.; Cui, X. Valley Polarization in MoS_2 Monolayers by Optical Pumping. *Nat. Nanotechnol.* **2012**, *7*, 490−493.

(24) Peng, B.; Yu, G.; Liu, X.; Liu, B.; Liang, X.; Bi, L.; Deng, L.; Sum, T. C.; Loh, K. P. Ultrafast Charge Transfer in MoS_2/WSe_2 P−N Heterojunction. *2D Mater.* **2016**, *3*, 025020.

(25) Zheng, J.; Zhang, H.; Dong, S.; Liu, Y.; Tai Nai, C.; Suk Shin, H.; Young Jeong, H.; Liu, B.; Loh, P. K. High Yield Exfoliation of Two-Dimensional Chalcogenides Using Sodium Naphthalenide. *Nat. Commun.* **2014**, *5*, 2995.

(26) Peng, B.; Yu, G.; Zhao, Y.; Xu, Q.; Xing, G.; Liu, X.; Fu, D.; Liu, B.; Tan, J. R. S.; Tang, W.; Lu, H.; Xie, J.; Deng, L.; Sum, T. C.; Loh, K. P. Achieving Ultrafast Hole Transfer at the Monolayer MoS_2 and $CH_3NH_3PbI_3$ Perovskite Interface by Defect Engineering. *ACS Nano* **2016**, *10*, 6383−6391.

(27) Liu, K. K.; Zhang, W. J.; Lee, Y. H.; Lin, Y. C.; Chang, M. T.; Su, C.; Chang, C. S.; Li, H.; Shi, Y. M.; Zhang, H.; Lai, C. S.; Li, L. J. Growth of Large-Area and Highly Crystalline MoS_2 Thin Layers on Insulating Substrates. *Nano Lett.* **2012**, *12*, 1538−1544.

(28) Ye, Z.; Cao, T.; O'Brien, K.; Zhu, H.; Yin, X.; Wang, Y.; Louie, S. G.; Zhang, X. Probing Excitonic Dark States in Single-Layer Tungsten Disulphide. *Nature* **2014**, *513*, 214−218.

(29) Zhang, C.; Wang, H.; Chan, W.; Manolatou, C.; Rana, F. Absorption of Light by Excitons and Trions in Monolayers of Metal Dichalcogenide MoS_2: Experiments and Theory. *Phys. Rev. B: Condens. Matter Mater. Phys.* **2014**, *89*, 205436.

(30) Mak, K. F.; He, K.; Lee, C.; Lee, G. H.; Hone, J.; Heinz, T. F.; Shan, J. Tightly Bound Trions in Monolayer MoS_2. *Nat. Mater.* **2013**, *12*, 207−211.

(31) He, K.; Kumar, N.; Zhao, L.; Wang, Z.; Mak, K. F.; Zhao, H.; Shan, J. Tightly Bound Excitons in Monolayer WSe_2. *Phys. Rev. Lett.* **2014**, *113*, 026803.

(32) Mak, K. F.; Lee, C.; Hone, J.; Shan, J.; Heinz, T. F. Atomically Thin MoS_2: A New Direct-Gap Semiconductor. *Phys. Rev. Lett.* **2010**, *105*, 136805.

(33) Kim, M. S.; Yun, S. J.; Lee, Y.; Seo, C.; Han, G. H.; Kim, K. K.; Lee, Y. H.; Kim, J. Biexciton Emission from Edges and Grain Boundaries of Triangular WS_2 Monolayers. *ACS Nano* **2016**, *10*, 2399−2405.

(34) Leroux, M.; Grandjean, N.; Beaumont, B.; Nataf, G.; Semond, F.; Massies, J.; Gibart, P. Temperature Quenching of Photoluminescence

DOI: 10.1021/acsnano.7b05743
ACS Nano 2017, 11, 12257−12265

Intensities in Undoped and Doped GaN. *J. Appl. Phys.* **1999**, *86*, 3721–3728.
(35) Cheiwchanchamnangij, T.; Lambrecht, W. R. L. Quasiparticle Band Structure Calculation of Monolayer, Bilayer, and Bulk MoS_2. *Phys. Rev. B: Condens. Matter Mater. Phys.* **2012**, *85*, 205302.
(36) Berkelbach, T. C.; Hybertsen, M. S.; Reichman, D. R. Theory of Neutral and Charged Excitons in Monolayer Transition Metal Dichalcogenides. *Phys. Rev. B: Condens. Matter Mater. Phys.* **2013**, *88*, 045318.
(37) Cudazzo, P.; Tokatly, I. V.; Rubio, A. Dielectric Screening in Two-Dimensional Insulators: Implications for Excitonic and Impurity States in Graphane. *Phys. Rev. B: Condens. Matter Mater. Phys.* **2011**, *84*, 085406.
(38) Lin, Y.; Ling, X.; Yu, L.; Huang, S.; Hsu, A. L.; Lee, Y. H.; Kong, J.; Dresselhaus, M. S.; Palacios, T. Dielectric Screening of Excitons and Trions in Single-Layer MoS_2. *Nano Lett.* **2014**, *14*, 5569–5576.
(39) Spivak, B.; Kravchenko, S. V.; Kivelson, S. A.; Gao, X. P. A. Transport in Strongly Correlated Two Dimensional Electron Fluid. *Rev. Mod. Phys.* **2010**, *82*, 1743–1766.
(40) Palummo, M.; Bernardi, M.; Grossman, J. C. Exciton Radiative Lifetimes in Two-Dimensional Transition Metal Dichalcogenides. *Nano Lett.* **2015**, *15*, 2794–2800.
(41) Zhu, B. R.; Zeng, H. L.; Dai, J. F.; Gong, Z. R.; Cui, X. D. Anomalously Robust Valley Polarization and Valley Coherence in Bilayer WS_2. *Proc. Natl. Acad. Sci. U. S. A.* **2014**, *111*, 11606–11611.
(42) Jin, C.; Kim, J.; Wu, K.; Chen, B.; Barnard, E. S.; Suh, J.; Shi, Z.; Drapcho, S. G.; Wu, J.; Schuck, P. J.; Tongay, S.; Wang, F. On Optical Dipole Moment and Radiative Recombination Lifetime of Excitons in WSe_2. *Adv. Funct. Mater.* **2017**, *27*, 1601741.
(43) Wang, H.; Zhang, C.; Chan, W.; Manolatou, C.; Tiwari, S.; Rana, F. Radiative Lifetimes of Excitons and Trions in Monolayers of the Metal Dichalcogenide MoS_2. *Phys. Rev. B: Condens. Matter Mater. Phys.* **2016**, *93*, 045407.
(44) Xu, X.; Zhao, Y.; Sie, E. J.; Lu, Y.; Liu, B.; Ekahana, S. A.; Ju, X.; Jiang, Q.; Wang, J.; Sun, H.; Sum, T. C.; Huan, C. H. A.; Feng, Y. P.; Xiong, Q. Dynamics of Bound Exciton Complexes in CdS Nanobelts. *ACS Nano* **2011**, *5*, 3660–3669.
(45) Kim, D.; Mishima, T.; Tomihira, K.; Nakayama, M. Temperature Dependence of Photoluminescence Dynamics in Colloidal CdS Quantum Dots. *J. Phys. Chem. C* **2008**, *112*, 10668–10673.
(46) Liang, X.; Zhu, Y.; Peng, B.; Deng, L.; Xie, J.; Lu, H.; Wu, M.; Bi, L. Influence of Interface Structure on Magnetic Proximity Effect in Pt/$Y_3Fe_5O_{12}$ Heterostructures. *ACS Appl. Mater. Interfaces* **2016**, *8*, 8175–8183.
(47) Li, C. Z.; Wang, L. X.; Liu, H.; Wang, J.; Liao, Z. M.; Yu, D. P. Giant Negative Magnetoresistance Induced by the Chiral Anomaly in Individual Cd_3As_2 Nanowires. *Nat. Commun.* **2015**, *6*, 10137.
(48) Li, H.; He, H.; Lu, H. Z.; Zhang, H.; Liu, H.; Ma, R.; Fan, Z.; Shen, S. Q.; Wang, J. Negative Magnetoresistance in Dirac Semimetal Cd_3As_2. *Nat. Commun.* **2016**, *7*, 10301.
(49) Li, Y.; Li, L.; Wang, J.; Wang, T.; Xu, X.; Xi, C.; Cao, C.; Dai, J. Resistivity Plateau and Negative Magnetoresistance in the Topological Semimetal $TaSb_2$. *Phys. Rev. B: Condens. Matter Mater. Phys.* **2016**, *94*, 121115.
(50) Li, Q.; Kharzeev, D. E.; Zhang, C.; Huang, Y.; Pletikosić, I.; Fedorov, A. V.; Zhong, R. D.; Schneeloch, J. A.; Gu, G. D.; Valla, T. Chiral Magnetic Effect in $ZrTe_5$. *Nat. Phys.* **2016**, *12*, 550.
(51) Huang, X.; Zhao, L.; Long, Y.; Wang, P.; Chen, D.; Yang, Z.; Liang, H.; Xue, M.; Weng, H.; Fang, Z.; Dai, X.; Chen, G. Observation of the Chiral-Anomaly-Induced Negative Magnetoresistance in 3D Weyl Semimetal TaAs. *Phys. Rev. X* **2015**, *5*, 031023.
(52) Zhang, E.; Chen, R.; Huang, C.; Yu, J.; Zhang, K.; Wang, W.; Liu, S.; Ling, J.; Wan, X.; Lu, H. Z.; Xiu, F. Tunable Positive to Negative Magnetoresistance in Atomically Thin WTe_2. *Nano Lett.* **2017**, *17*, 878–885.
(53) Wu, H. C.; Chaika, A. N.; Hsu, M.-C.; Huang, T. W.; Abid, M.; Abid, M.; Aristov, V. Y.; Molodtsova, O. V.; Babenkov, S. V.; Niu, Y.; Murphy, B. E.; Krasnikov, S. A.; Lübben, O.; Liu, H.; Chun, B. S.; Janabi, Y. T.; Molotkov, S. N.; Shvets, I. V.; Lichtenstein, A. I.; Katsnelson, M. I.; et al. Large Positive In-Plane Magnetoresistance Induced by Localized States at Nanodomain Boundaries in Graphene. *Nat. Commun.* **2017**, *8*, 14453.
(54) Jie, W.; Yang, Z.; Zhang, F.; Bai, G.; Leung, C. W.; Hao, J. Observation of Room-Temperature Magnetoresistance in Monolayer MoS_2 by Ferromagnetic Gating. *ACS Nano* **2017**, *11*, 6950–6958.
(55) Sun, Y.; Chang, H.; Kabatek, M.; Song, Y. Y.; Wang, Z.; Jantz, M.; Schneider, W.; Wu, M.; Montoya, E.; Kardasz, B.; Heinrich, B.; Te Velthuis, S. G. E.; Schultheiss, H.; Hoffmann, A. Damping in Yttrium Iron Garnet Nanoscale Films Capped by Platinum. *Phys. Rev. Lett.* **2013**, *111*, 106601.
(56) Mak, K. F.; McGill, K. L.; Park, J.; McEuen, P. L. The Valley Hall Effect in MoS_2 Transistors. *Science* **2014**, *344*, 1489–1492.
(57) Kajiwara, Y.; Harii, K.; Takahashi, S.; Ohe, J.; Uchida, K.; Mizuguchi, M.; Umezawa, H.; Kawai, H.; Ando, K.; Takanashi, K.; Maekawa, S.; Saitoh, E. Transmission of Electrical Signals by Spin-Wave Interconversion in a Magnetic Insulator. *Nature* **2010**, *464*, 262–266.
(58) Jungwirth, T.; Wunderlich, J.; Olejnik, K. Spin Hall Effect Devices. *Nat. Mater.* **2012**, *11*, 382–390.
(59) Qiu, Z.; Li, J.; Hou, D.; Arenholz, E.; N'Diaye, A. T.; Tan, A.; Uchida, K. I.; Sato, K.; Okamoto, S.; Tserkovnyak, Y.; Qiu, Z. Q.; Saitoh, E. Spin-Current Probe for Phase Transition in an Insulator. *Nat. Commun.* **2016**, *7*, 12670.

DOI: 10.1021/acsnano.7b05743
ACS Nano 2017, 11, 12257–12265